Collisional Relaxation of Fine Velocity Structures in Plasmas

Oreste Pezzi, Francesco Valentini, and Pierluigi Veltri
Dipartimento di Fisica, Università della Calabria, 87036 Rende (CS), Italy
(Received 19 November 2015; published 5 April 2016)

The existence of several characteristic times during the collisional relaxation of fine velocity structures is investigated by means of Eulerian numerical simulations of a spatially homogeneous force-free weakly collisional plasma. The effect of smoothing out velocity gradients on the evolution of global quantities, such as temperature and entropy, is discussed, suggesting that plasma collisionality can locally increase due to velocity space deformations of the particle velocity distribution function. These results support the idea that high-resolution measurements of the particle velocity distribution function are crucial for an accurate description of weakly collisional systems, such as the solar wind, in order to answer relevant scientific questions, related, for example, to particle heating and energization.

DOI: 10.1103/PhysRevLett.116.145001

The description of collisional effects in plasmas represents historically a huge scientific topic in which a significant numerical and theoretical effort has been made even in recent years [1–8]. In a weakly collisional plasma, such as the solar wind, collisions are usually considered far too weak to produce any significant effect on the plasma dynamics [9]. However, the estimation of collisionality is often based on the restrictive assumption that the shape of the particle velocity distribution function (VDF) is close to Maxwellian [10–12]. On the other hand, kinetic simulations [13–20], as well as *in situ* spacecraft measurements in the solar wind (SW) [12,21–24], indicate that marked non-Maxwellian features develop in the three-dimensional VDFs (temperature anisotropies, particle beams, ringlike modulations, etc.). Fine velocity structures naturally form in a kinetic plasma when an initial inhomogeneity is let free to evolve (ballistic effect) [25,26]. Nonlinear wave-particle interactions can lead in addition to larger scale velocity structures possibly taking part in a kinetic turbulent cascade and/or to instabilities. Since collisional effects increase with the velocity gradients of the VDF [27–33], the collisionless hypothesis may locally fail.

Velocity space structures can store the VDF free energy [34], which is then available for wave production through microinstabilities or for heating production due to collisional thermalization, which generates a degradation of information, i.e., an entropy production. Hence, investigating the role of collisions on small scale velocity space structures is relevant for understanding how collisionless wave-particle interactions compete with collisional processes and how efficiently collisions can be enhanced by the presence of fine velocity space gradients and play a significant role in converting ordered energy into heat. To highlight this effect, it is mandatory to adopt nonlinear collisional operators where the strength of the collisional terms depends on the VDFs shape. Up to now, collisional effects have been almost always modeled through simplified operators [35–40], which are linear or assume a reduced dimensionality in velocity space.

On the contrary, we modeled collisions through the full Landau operator, which is a nonlinear integro-differential operator of the Fokker-Planck type, has good conservation properties, and satisfies an H-theorem for the Gibbs-Boltzmann entropy [27,28]. The Landau operator introduces an upper cutoff of the integrals at the Debye length to mimic the effects of the time correlations due to the eigenmodes and so avoid divergence at large scale. A more general treatment of collisions (Balescu-Lenard operator [29,30]), which introduces the eigenmodes in a more consistent way through the dispersion equation, is much more difficult to manage numerically.

In this Letter, we discuss the collisional dissipation of non-Maxwellian features in the particle VDFs in a weakly collisional plasma, by means of Eulerian numerical simulations. Because of the nonlinear nature of the Landau operator, the analytical treatment as well as the self-consistent numerical simulations of the Landau operator in 6D phase space are difficult goals to achieve yet. Thus, we decided to address the collisional relaxation of a spatially homogeneous force-free plasma and to model collisions between particles of the same species through the following (dimensionless) collisional evolution equation for the particle distribution function $f(\mathbf{v})$:

$$\frac{\partial f(\mathbf{v})}{\partial t} = \pi \left(\frac{3}{2}\right)^{\frac{3}{2}} \frac{\partial}{\partial v_i} \int d^3 v' U_{ij}(\mathbf{u}) \times \left[f(\mathbf{v}') \frac{\partial f(\mathbf{v})}{\partial v_j} - f(\mathbf{v}) \frac{\partial f(\mathbf{v}')}{\partial v'_j} \right], \quad (1)$$

being f normalized such that $\int d^3 v f(\mathbf{v}) = n = 1$ and $U_{ij}(\mathbf{u})$

$$U_{ij}(\mathbf{u}) = \frac{\delta_{ij} u^2 - u_i u_j}{u^3}, \quad (2)$$

where $\mathbf{u} = \mathbf{v} - \mathbf{v}'$, $u = |\mathbf{u}|$ and the Einstein notation is introduced. In Eq. (1), and from now on, time is scaled to the inverse Spitzer-Harm frequency ν_{SH}^{-1} [10] and velocity to the particle thermal speed v_{th}. Details about the numerical solution of Eq. (1) can be found in Ref. [3].

In the first part of the present Letter, we consider the mutual effect of a local deformation of the particle VDF (a plateau) and the global temperature anisotropy, by comparing the evolution of two initial VDFs:

$$f_1(\mathbf{v}) = C_1 f_{M,T_\perp}(v_x) f_{M,T_\perp}(v_y) f_{p,T_\parallel}(v_z), \quad (3)$$

$$f_2(\mathbf{v}) = C_2 f_{M,T_\perp}(v_x) f_{M,T_\perp}(v_y) f_{M,T_\parallel}(v_z), \quad (4)$$

where C_1 and C_2 are normalization constants. The total temperature T, where $T = v_{th}^2$ in dimensionless units, is given by $T = (T_\parallel + 2T_\perp)/3$ and $A = T_\perp/T_\parallel = 2$. Finally f_{M,T_i} is a generic Maxwellian with temperature T_i and [2,4]:

$$f_{p,T_\parallel}(v_z) = f_{M,T_0}(v_z) - \frac{f_{M,T_0}(v_z) - f_{M,T_0}(V_0)}{1 + [(v_z - V_0)/\Delta V_p]^{n_p}} \quad (5)$$

where $T_0 = 1$, $V_0 = 1.44$, $\Delta V_p = 0.5$, and $n_p = 8$. The function $f_{p,T_\parallel}(v_z)$ is constructed in such a way to have a plateau of width ΔV_p around $v = V_0$, that is $f'_{p,T\parallel}(v_z)$ is about null in the interval $V_0 - \Delta V_p/2 \lesssim v_z \lesssim V_0 + \Delta V_p/2$, being exactly zero at $v_z = V_0$.

It is worth to note that $f_2(\mathbf{v})$ is a bi-Maxwellian function, while $f_1(\mathbf{v})$ is Maxwellian in the perpendicular directions with a plateau centered in $v_z = V_0$ in the parallel direction. We also point out that $f_1(\mathbf{v})$ and $f_2(\mathbf{v})$ have the same temperature (second order moment) in each direction. Moreover, for the function $f_1(\mathbf{v})$, we reset the small mean velocity ($\simeq 10^{-2}$) produced by the presence of the plateau. The three-dimensional velocity domain is discretized with $N_{v_x} = N_{v_y} = 51$ and $N_{v_z} = 1601$ grid points. We point out that the resolution along v_z has been increased significantly in order to resolve the short velocity scales associated with the presence of the plateau. Finally, the distribution function is set equal to zero for $|v_j| > v_{\max} = 6v_{th}$, being $j = x, y, z$.

As shown in Fig. 1(a), the time evolution of parallel and perpendicular temperatures of $f_1(\mathbf{v})$ (black solid line) and $f_2(\mathbf{v})$ (red dashed line) is clearly the same. On the other hand, the evolution of the entropy variation $\Delta S = S(t) - S(0)$ ($S = -\int f \ln f d^3v$), reported in Fig. 1(b), displays significant differences. In particular, for $f_1(\mathbf{v})$ (black solid curve), the case in which a plateau is present, ΔS saturates at a larger level than that recovered for $f_2(\mathbf{v})$ (red dashed curve). In order to investigate the reasons of such different behavior of the entropy for $f_1(\mathbf{v})$ and $f_2(\mathbf{v})$, we performed a multiexponential fit [41] of ΔS for the two cases, with the following curve:

$$\Delta S(t) = \sum_{i=1}^{K} \Delta S_i (1 - e^{-t/\tau_i}), \quad (6)$$

τ_i being the ith characteristic time and K is evaluated through a recursive procedure.

From this analysis, we found that, while for the case of $f_2(\mathbf{v})$ [red dashed curve of Fig. 1(b)] ΔS shows an exponential growth with a single characteristic time ($\tau \simeq 2\nu_{SH}^{-1}$), for $f_1(\mathbf{v})$ [black solid curve of Fig. 1(b)], i.e., in the presence of a plateau, two different characteristic times are recovered: a fast characteristic time $\tau_1 = 0.14\nu_{SH}^{-1}$ [indicated in Figs. 1(a) and 1(b) by a vertical blue dashed line] in which 25% of the total entropy growth is achieved, and a slow characteristic time $\tau_2 = 2.03\nu_{SH}^{-1}$ during which the remaining 75% of the total entropy growth is observed. We argue that the existence of the characteristic time τ_1 is due to the presence of the plateau, and in particular it is associated with the sharp velocity gradients in $f_1(\mathbf{v})$, while τ_2 is related to the initial temperature anisotropy. In fact, as it can be seen in Fig. 1(c) where $f_1(v_x = v_y = 0, v_z)$ is plotted as a function of v_z at $t = 0$ (black solid line) and at $t = \tau_1$ (red dashed line), the initial plateau is completely smoothed out by collisional effects in a time close to τ_1, while from Fig. 1(a) one realizes that at $t \simeq \tau_1$ the temperature anisotropy is still present.

To further support the idea that the presence of sharp velocity gradients in the particle VDF causes the entropy to grow over different time scales, we made an additional numerical experiment of collisional relaxation, considering a different initial condition for Eq. (1). This new initial condition has been designed as follows. First, we performed a 1D-1V Vlasov-Poisson simulation (kinetic electrons and motionless protons) with high numerical

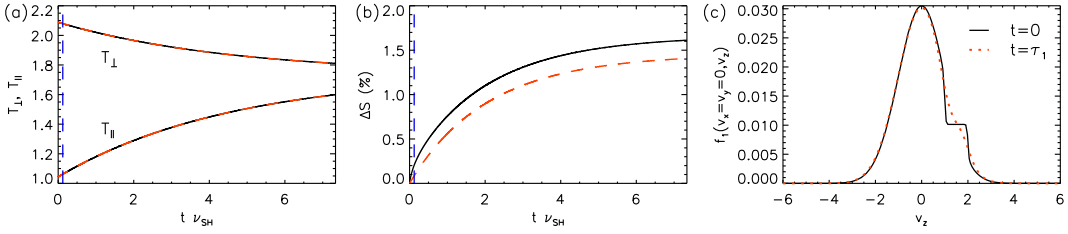

FIG. 1. (a) Time evolution of $T_\perp$ and $T_\parallel$ for the case of $f_1(\mathbf{v})$ (black solid line) and $f_2(\mathbf{v})$ (red dashed line). (b) Time evolution of ΔS for the case of $f_1(\mathbf{v})$ (black solid line) and $f_2(\mathbf{v})$ (red dashed line). The vertical blue dashed line in panels (a)–(b) indicates the time instant $t = \tau_1$. (c) Distribution function $f_1(v_x = v_y = 0, v_z)$ as a function of v_z at $t = 0$ (black solid line) and at $t = \tau_1$ (red dashed line).

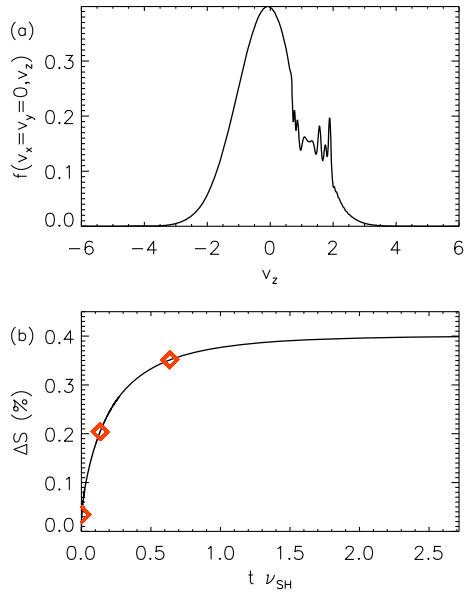

FIG. 2. (a) Dependence of f on v_z. (b) Time history of ΔS. Red diamonds in panel (b) indicate the time instants $t = \tau_1$, $t = \tau_1 + \tau_2$, $t = \tau_1 + \tau_2 + \tau_3$.

resolution in the $z - v_z$ phase space domain ($N_z = 256$, $N_{v_z} = 1601$). In this simulation, we externally forced the system, initially at equilibrium, through a sinusoidal driver electric field, in order to excite a large amplitude electron acoustic wave (EAW) [42], as it has been done numerically in Refs. [43–45] and in laboratory experiments with non-neutral plasmas in Refs. [46,47]. As discussed in these papers, the propagation of large amplitude EAWs is characterized by the generation of phase space structures of the Bernstein-Green-Kruskal (BGK) type [48] in the electron distribution function $f_e(z, v_z)$, associated with trapped particle populations. Then, we selected the spatial point z_0 in the numerical domain, where this BGK-like phase space structure displays its maximum velocity width, and considered the velocity profile $\hat{f}_e(v_z) = f_e(z_0, v_z)$. In Fig. 2(a), we report the dependence of $\hat{f}_e$ on v_z; here, it can be appreciated that $\hat{f}_e$ is highly distorted due to nonlinear wave-particle interaction processes and displays the presence of sharp velocity gradients (bumps, holes, spikes, etc.). At this point, we evaluated the second-order velocity moment of $\hat{f}_e$, that is the temperature T_e, and built up the three-dimensional VDF $f(v_x, v_y, v_z) = f_{M,T_e}(v_x) f_{M,T_e}(v_y) \hat{f}_e(v_z)$. We emphasize that this VDF has the same temperature in each velocity direction but presents strong non-Maxwellian deformations along v_z, as shown in Fig. 2(a), which make the system far from equilibrium. The time history of ΔS, obtained when using f as initial condition for Eq. (1), is presented in Fig. 2(b). As in the previous simulations, the three-dimensional velocity domain in this case is discretized by $N_{v_x} = N_{v_y} = 51$ and $N_{v_z} = 1601$ grid points.

By analyzing the entropy growth through the same method of multiexponential fit discussed previously, three characteristic times are recovered in this case, whose values are reported below, together with the corresponding percentage of entropy variation: (i) $\tau_1 = 3.5 \times 10^{-3} \nu_{SH}^{-1} \rightarrow \Delta S_1/\Delta S_{\rm tot} = 13\%$, (ii) $\tau_2 = 1.3 \times 10^{-1} \nu_{SH}^{-1} \rightarrow \Delta S_2/\Delta S_{\rm tot} = 42\%$, (iii) $\tau_3 = 4.9 \times 10^{-1} \nu_{SH}^{-1} \rightarrow \Delta S_3/\Delta S_{\rm tot} = 40\%$.

Characteristic times τ_1, τ_2, and τ_3 are indicated as red diamonds in Fig. 2(b). In Fig. 3, we plot f as a function of v_z for $v_x = v_y = 0$, at three different times $t = \tau_1$ (a), $t = \tau_1 + \tau_2$ (b), and $t = \tau_1 + \tau_2 + \tau_3$ (c): during the time τ_1, steep spikes visible in Fig. 2(a) are almost completely smoothed out; at time $\tau_1 + \tau_2$ the remaining plateau region is significantly rounded off, only a gentle shoulder being left; finally, after a time $\tau_1 + \tau_2 + \tau_3$, the collisional return to equilibrium is completed for the most part (a small percentage $\simeq 5\%$ of the total entropy growth is finally recovered for larger times and corresponds to the final approach to the equilibrium Maxwellian, indicated by red dashed lines in the three panels of Fig. 3).

Compared to the case shown in Fig. 1, here we recovered an additional extremely fast characteristic time ($\simeq 10^{-3} \nu_{SH}^{-1}$), associated with the sharp velocity gradients of f along v_z, while we did not detect the large characteristic time ($\simeq 2\nu_{SH}^{-1}$) associated with the temperature anisotropy in the previous case.

Numerical experiments discussed so far give a clear message: collisional dissipation of small velocity scales in the particle VDF occurs over different characteristic times, inversely proportional to the sharpness of the velocity gradients associated with those velocity scales. As we discussed above, these characteristic times can be significantly smaller than the Spitzer-Harm collisional time [10],

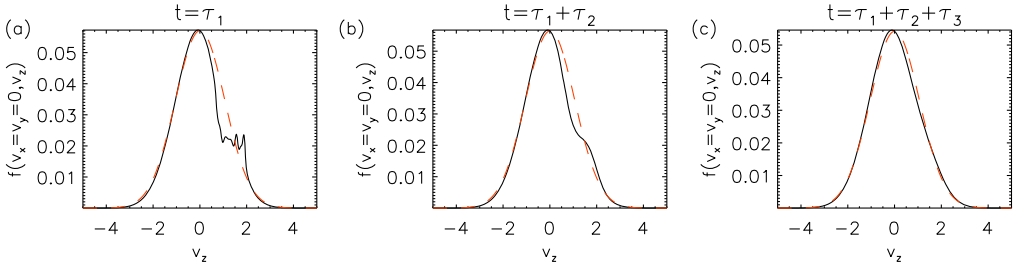

FIG. 3. Distribution function $f(v_x = 0, v_y = 0, v_z)$ as a function of v_z at $t = \tau_1$ (a), $t = \tau_1 + \tau_2$ (b), and $t = \tau_1 + \tau_2 + \tau_3$ (c). Red dashed lines in panels (a)–(c) indicate the equilibrium Maxwellian finally reached in the simulation.

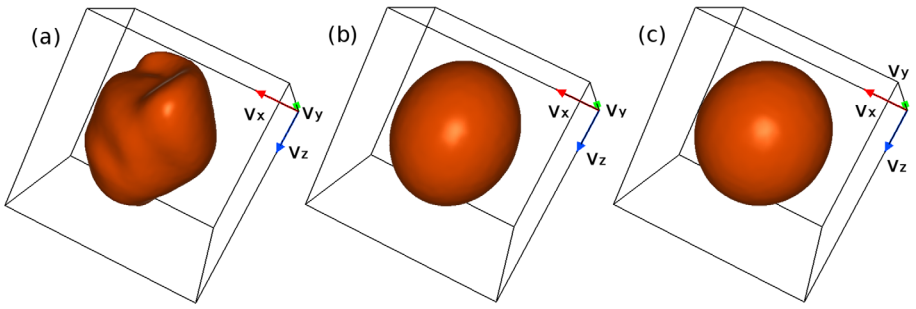

FIG. 4. Iso-surface plot of the initial VDFs $f_{sw}(\mathbf{v})$ (a), $\tilde{f}_{sw}(\mathbf{v})$ (b), and $\hat{f}_{sw}(\mathbf{v})$ (c), respectively.

this meaning that the presence of velocity gradients in fact speeds up the growth of the entropy of the system. This evidence suggests that when the particle VDFs exhibit small velocity scale deformations, the quasi-Maxwellian approximation, on which the Spitzer-Harm collisional evolution is based, is no longer appropriate.

In order to explore the implications of our results to the general case of the SW plasma, we performed our analysis on a three-dimensional proton VDF $f_{sw}(\mathbf{v})$, obtained from the hybrid Vlasov-Maxwell [49] numerical simulations of SW decaying turbulence described in detail in Refs. [15–20]. As shown in Fig. 4(a), where the three-dimensional iso-surface plot of f_{sw} is reported, kinetic effects along the cascade make the VDF depart from the spherical shape of Maxwellian equilibrium and resemble a deformed potato. Then, having in mind to mimic low resolution VDF measurements by a real spacecraft, we fitted $f_{sw}(\mathbf{v})$ with a tri-Maxwellian function $\tilde{f}_{sw}(\mathbf{v})$ [Fig. 4(b)] and with a bi-Maxwellian function $\hat{f}_{sw}(\mathbf{v})$ [Fig. 4(c)]. In order to point out the loss of physical information caused by not adequately resolving the sharp velocity gradients in the particle VDFs, the functions f_{sw}, $\tilde{f}_{sw}$, and $\hat{f}_{sw}$ are used as initial conditions in three new simulations of Eq. (1), in which the velocity domain is now discretized by $N_{v_x} = N_{v_y} = N_{v_z} = 51$ grid points, as in the simulations in Refs. [15–20]. The results for the entropy growth of these new numerical experiments are reported in Fig. 5, where we show the time evolution of ΔS for the VDFs $f_{sw}(\mathbf{v})$ (black solid line), $\tilde{f}_{sw}(\mathbf{v})$ (red dashed line), and $\hat{f}_{sw}(\mathbf{v})$ (blue dashed line), respectively.

As for the previous cases discussed above, also here the time history of ΔS is evidently affected by the presence of fine velocity scales and steep gradients in the particle VDF. Any fitting procedure, which smooths out the fine velocity structures, reduces the entropy growth: in fact, the simulation with the function $\hat{f}_{sw}(\mathbf{v})$ as initial condition displays a collisional entropy growth about 20 times smaller than that recovered for the case of the function $f_{sw}(\mathbf{v})$. Moreover, through the multiexponential fit analysis performed on ΔS for the simulation initialized with f_{sw}, we found two characteristic times: a fast one $\tau_1 = 0.20\nu_{SH}^{-1}$, in which 26% of the total entropy growth is achieved, and a slow one $\tau_2 = 0.82\nu_{SH}^{-1}$, during which the remaining 74% of the total entropy growth is observed. By analyzing VDF iso-surface plots (not shown here) at different times in the simulation, we realized that after a time $t = \tau_1$ collisions have dissipated most of the sharp velocity gradients which were initially present in the VDF. We point out that, since the numerical resolution for this simulation is about 30 times smaller than in the previous case, sharp velocity gradients [as those shown in Fig. 2(a)] are not visible in the particle VDF, even though it displays significant non-Maxwellian features [see Fig. 4(a)]. Hence, the lack of velocity resolution presumably does not allow us to recover the extremely fast characteristic time ($\simeq 10^{-3}\nu_{SH}^{-1}$) in the evolution of ΔS, observed for the simulation initialized with the velocity profile in Fig. 2(a).

In this Letter, we discussed the role of the VDF fine velocity structures in enhancing the plasma collisionality. In particular, by means of Eulerian simulations of collisional relaxation of a spatially homogeneous force-free plasma, we have shown that the system entropy growth occurs over several time scales, which gets smaller as VDF gradients become steeper. We reported clear evidences that these gradients are dissipated by collisions in a time much shorter than that associated with global non-Maxwellian features, e.g., temperature anisotropies. This characteristic time may be comparable or even smaller than the instability growth rates invoked to explain the SW anisotropic VDFs [50,51] or than the nonlinear dynamics times, as recently discussed through a classical treatment of collisions [8].

We finally pointed out how the lack of resolution in the VDFs measurements mask a relevant part of physical

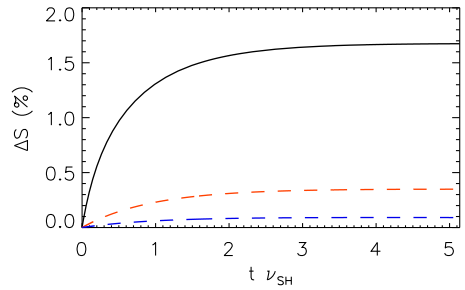

FIG. 5. Entropy growth for the initial VDFs $f_{sw}(\mathbf{v})$ (black line), $\tilde{f}_{sw}(\mathbf{v})$ (red dashed line), and $\hat{f}_{sw}(\mathbf{v})$ (blue dashed line), respectively.

information hidden in the sharp velocity gradients of the non-Maxwellian VDFs, observed ubiquitous, for example, in the SW [21,24]. Future space missions, planned to increase both energy and angular resolutions of the VDFs measurements, will provide crucial insights for the long-standing problems of plasma heating and particle energization in the interplanetary medium.

Numerical simulations here discussed have been run on the Fermi parallel machine at Cineca (Italy), within the project COLTURBO—HP10CVRU0Q. This work has been supported by the Agenzia Spaziale Italiana under the Contract No. ASI-INAF 2015-039-R.O "Missione M4 di ESA: Partecipazione Italiana alla fase di assessment della missione THOR."

[1] O. Pezzi, F. Valentini, D. Perrone, and P. Veltri, Phys. Plasmas **20**, 092111 (2013).
[2] O. Pezzi, F. Valentini, D. Perrone, and P. Veltri, Phys. Plasmas **21**, 019901 (2014).
[3] O. Pezzi, F. Valentini, and P. Veltri, J. Plasma Phys. **81**, 305810107 (2015).
[4] O. Pezzi, F. Valentini, and P. Veltri, Phys. Plasmas **22**, 042112 (2015).
[5] F. Filbet and L. Pareschi, J. Comput. Phys. **179**, 1 (2002).
[6] A. V. Bobylev and I. F. Potapenko, J. Comput. Phys. **246**, 123 (2013).
[7] D. F. Escande, Y. Elskens, and F. Doveil, J. Plasma Phys. **81**, 305810101 (2015).
[8] S. F. Tigik, L. F. Ziebell, P. H. Yoon, and E. P. Kontar, Astron. Astrophys. **586**, A19 (2016).
[9] R. Bruno and V. Carbone, Living Rev. Solar Phys. **10**, 1 (2013).
[10] L. Spitzer Jr., *Physics of Fully Ionized Gases* (Interscience Publishers, New York, 1956).
[11] R. Hernandez and E. Marsch, J. Geophys. Res. **90**, 11062 (1985).
[12] B. A. Maruca, S. D. Bale, L. Sorriso-Valvo, J. C. Kasper, and M. L. Stevens, Phys. Rev. Lett. **111**, 241101 (2013).
[13] F. Valentini, F. Califano, D. Perrone, F. Pegoraro, and P. Veltri, Phys. Rev. Lett. **106**, 165002 (2011).
[14] D. Perrone, F. Valentini, and P. Veltri, Astrophys. J. **741**, 43 (2011).
[15] S. Servidio, F. Valentini, F. Califano, and P. Veltri, Phys. Rev. Lett. **108**, 045001 (2012).
[16] A. Greco, F. Valentini, S. Servidio, and W. H. Matthaeus, Phys. Rev. E **86**, 066405 (2012).
[17] D. Perrone, F. Valentini, S. Servidio, S. Dalena, and P. Veltri, Astrophys. J. **762**, 99 (2013).
[18] S. Servidio, K. T. Osman, F. Valentini, D. Perrone, F. Califano, S. Chapman, W. H. Matthaeus, and P. Veltri, Astrophys. J. Lett. **781**, L27 (2014).
[19] S. Servidio, F. Valentini, D. Perrone, A. Greco, F. Califano, W. H. Matthaeus, and P. Veltri, J. Plasma Phys. **81**, 325810107 (2015).
[20] F. Valentini, S. Servidio, D. Perrone, F. Califano, W. H. Matthaeus, and P. Veltri, Phys. Plasmas **21**, 082307 (2014).
[21] E. Marsch, Living Rev. Solar Phys. **3**, 1 (2006).
[22] J. C. Kasper, A. J. Lazarus, and S. P. Gary, Phys. Rev. Lett. **101**, 261103 (2008).
[23] B. A. Maruca, J. C. Kasper, and S. D. Bale, Phys. Rev. Lett. **107**, 201101 (2011).
[24] J. Je, L. Wang, C. Tu, E. Marsch, and Q. Zong, Astrophys. J. Lett. **800**, L31 (2015).
[25] G. Belmont, F. Mottez, T. Chust, and S. Hess, Phys. Plasmas **15**, 052310 (2008).
[26] T. Chust, G. Belmont, F. Mottez, and S. Hess, Phys. Plasmas **16**, 092104 (2009).
[27] L. D. Landau, Phys. Z. Sowjet. **10**, 154 (1936); translated in The transport equation in the case of the Coulomb interaction, *Collected Papers of L. D. Landau* (Pergamon Press, Oxford, 1981).
[28] M. N. Rosenbluth, W. M. MacDonald, and D. L. Judd, Phys. Rev. **107**, 1 (1957).
[29] A. Lenard, Ann. Phys. (N.Y.) **10**, 390 (1960).
[30] R. Balescu, Phys. Fluids **3**, 52 (1960).
[31] T. H. Jensen, J. H. Malmberg, and T. M. O'Neil, Phys. Fluids **12**, 1728 (1969).
[32] A. I. Akhiezer, I. A. Akhiezer, R. V. Polovin, A. G. Sitenko, and K. N. Stepanov, *Plasma Electrodynamics* (Pergamon Press, Oxford, 1975), Vol. 1.
[33] R. L. Liboff, *Kinetic Theory: Classical, Quantum, and Relativistic Descriptions* (Springer, New York, 2003).
[34] M. Lesur, P. H. Diamond, and Y. Kosuga, Phys. Plasmas **21**, 112307 (2014).
[35] A. Lenard and I. B. Bernstein, Phys. Rev. **112**, 1456 1958).
[36] V. E. Zakharov and V. I. Karpman, Sov. Phys. JETP **16**, 351 (1963).
[37] J. P. Dougherty, Phys. Fluids **7**, 1788 (1964).
[38] J. P. Dougherty and S. R. Watson, J. Plasma Phys. **1**, 317 (1967).
[39] T. M. O'Neil, Phys. Fluids **11**, 2420 (1968).
[40] M. W. Anderson and T. M. O'Neil, Phys. Plasmas **14**, 112110 (2007).
[41] L. J. Curtis, H. G. Berry, and J. Bromander, Phys. Scr. **2**, 216 (1970).
[42] J. P. Holloway and J. J. Dorning, Phys. Rev. A **44**, 3856 (1991).
[43] F. Valentini, T. M. O'Neil, and D. H. E. Dubin, Phys. Plasmas **13**, 052303 (2006).
[44] T. W. Johnston, Y. Tyshetskiy, A. Ghizzo, and P. Bertrand, Phys. Plasmas **16**, 042105 (2009).
[45] F. Valentini, D. Perrone, F. Califano, F. Pegoraro, P. Veltri, P. J. Morrison, and T. M. O'Neil, Phys. Plasmas **19**, 092103 (2012).
[46] A. A. Kabantsev, F. Valentini, and C. Fred Driscoll, AIP Conf. Proc. **862**, 13 (2006).
[47] F. Anderegg, C. F. Driscoll, D. H. E. Dubin, and T. M. O'Neil, Phys. Rev. Lett. **102**, 095001 (2009).
[48] I. B. Bernstein, J. M. Greene, and M. D. Kruskal, Phys. Rev. **108**, 546 (1957).
[49] F. Valentini, P. Trávníček, F. Califano, P. Hellinger, and A. Mangeney, J. Comput. Phys. **225**, 753 (2007).
[50] W. H. Matthaeus, S. Oughton, K. T. Osman, S. Servidio, M. Wan, S. P. Gary, M. A. Shay, F. Valentini, V. Roytershteyn, and H. Karimabadi, Astrophys. J. **790**, 155 (2014).
[51] S. P. Gary, *Theory of Space Plasma Microinstabilities* (Cambridge University Press, New York, 1993).